

# 1 Deriving in situ phytoplankton absorption for bio-optical productivity 2 models in turbid waters

3 Matthew J. Oliver, Oscar Schofield, Trisha Bergmann, and Scott Glenn  
4 Institute of Marine and Coastal Sciences, Rutgers University, New Brunswick, New Jersey, USA

5 Cristina Orrico and Mark Moline  
6 Biological Sciences Department, California Polytechnic State University, San Luis Obispo, California, USA

7 Received 5 September 2002; revised 28 April 2003; accepted 25 July 2003; published XX Month 2004.

8 [1] As part of Hyperspectral Coupled Ocean Dynamics Experiment, a high-resolution  
9 hydrographic and bio-optical data set was collected from two cabled profilers at the Long-  
10 Term Ecosystem Observatory (LEO). Upwelling- and downwelling-favorable winds and a  
11 buoyant plume from the Hudson River induced large changes in hydrographic and optical  
12 structure of the water column. An absorption inversion model estimated the relative  
13 abundance of phytoplankton, colored dissolved organic matter (CDOM) and detritus, as  
14 well as the spectral exponential slopes of CDOM and detritus from in situ WET Labs nine-  
15 wavelength absorption/attenuation meter (ac-9) absorption data. Derived optical weights  
16 were proportional to the parameter concentrations and allowed for their absorptions to  
17 be calculated. Spectrally weighted phytoplankton absorption was estimated using modeled  
18 spectral irradiances and the phytoplankton absorption spectra inverted from an ac-9.  
19 Derived mean spectral absorption of phytoplankton was used in a bio-optical model  
20 estimating photosynthetic rates. Measured radiocarbon uptake productivity rates  
21 extrapolated with water mass analysis and the bio-optical modeled results agreed within  
22 20%. This approach is impacted by variability in the maximum quantum yield ( $\phi_{\max}$ ) and  
23 the irradiance light-saturation parameter ( $E_{k(\text{PAR})}$ ). An analysis of available data shows that  
24  $\phi_{\max}$  variability is relatively constrained in temperate waters. The variability of  $E_{k(\text{PAR})}$   
25 is greater in temperate waters, but based on a sensitivity analysis, has an overall smaller  
26 impact on water-column-integrated productivity rates because of the exponential decay of  
27 light. This inversion approach illustrates the utility of bio-optical models in turbid coastal  
28 waters given the measurements of the bulk inherent optical properties. *INDEX TERMS:*  
29 4853 Oceanography: Biological and Chemical: Photosynthesis; 4847 Oceanography: Biological and  
30 Chemical: Optics; 4552 Oceanography: Physical: Ocean optics; 4842 Oceanography: Biological and  
31 Chemical: Modeling; 4894 Oceanography: Biological and Chemical: Instruments and techniques; *KEYWORDS:*  
32 coastal, productivity, optics

33 **Citation:** Oliver, M. J., O. Schofield, T. Bergmann, S. Glenn, C. Orrico, and M. Moline (2004), Deriving in situ phytoplankton  
34 absorption for bio-optical productivity models in turbid waters, *J. Geophys. Res.*, 109, C07S11, doi:10.1029/2002JC001627.

## 36 1. Introduction

37 [2] There is growing evidence that anthropogenic-  
38 induced changes to the coastal ocean are increasing and  
39 will continue to do so as coastal regions are developed  
40 worldwide [Hallegraeff, 1993]. This is significant as the  
41 coastal ocean represents a significant fraction of the total  
42 ocean productivity [Field *et al.*, 1998; Bienfang and  
43 Ziemann, 1992], produces 90% of the global fish catch  
44 [Holligan and Reiners, 1992], and acts as a nutrient buffer  
45 between the terrestrial ecosystems and the open ocean  
46 [Biscaye *et al.*, 1994; Falkowski *et al.*, 1994]. Despite the  
47 functional importance of the coastal ocean, our understand-  
48 ing of physical and biological processes in nearshore coastal

waters (<30 m deep) is severely limited due to its highly  
49 turbulent nature [Brink, 1997]. Therefore there is a need to  
50 develop effective means to map biological and chemical  
51 processes in coastal ecosystems. 52

[3] Optical techniques are more commonly being used to  
53 assess spatial and temporal phytoplankton dynamics of  
54 offshore waters [cf. Advances in Ocean Optics, *Journal*  
55 *of Geophysical Research*, 100(C7), 13,133–13,372, 1995];  
56 however, these approaches are often compromised because  
57 of the optical complexity of coastal waters. For example,  
58 ocean color satellite chlorophyll algorithms are based on  
59 ratios of remote sensing reflectance ( $R_{rs}$ ) at different wave-  
60 lengths. Most satellite algorithms assume that  $R_{rs}$  patterns  
61 are based on case 1 waters where the in situ absorption  
62 and water-leaving radiance ( $L_w$ ) signal in the blue wave-  
63 lengths are dominated by chlorophyll absorption while  $L_w$   
64 in the green wavelengths is relatively insensitive to chloro- 65

66 phyll concentrations [Gordon and Morel, 1983]. Inaccuracies  
67 in this approach arise in coastal waters that contain  
68 significant amounts of other absorbing/scattering com-  
69 pounds such as dissolved organics, detritus, and even  
70 variable phytoplankton communities [Morel and Prieur,  
71 1977; T. Bergmann et al., The impacts of a recurrent  
72 resuspension event and variable phytoplankton community  
73 composition on remote sensing reflectance, submitted to  
74 *Journal of Geophysical Research*, 2002]. These errors  
75 directly impact the utility of optical techniques for  
76 estimating primary production and in turn impacts our  
77 understanding of carbon flux and nutrient recycling in  
78 nearshore ecosystems and their relation to ecosystem  
79 function [Jickells, 1998; Cloern, 2001].

80 [4] Resolving the impact of primary production on any  
81 oceanic system is ultimately a question of scale [Bidigare  
82 et al., 1992], which has been recently addressed with  
83 comparisons of local, regional, and global productivity  
84 models in ocean observatories. Comparisons of modeled  
85 and measured primary production in these observatories  
86 showed mixed results. For example, satellite-based depth-  
87 integrated models [see Behrenfeld and Falkowski, 1997 for  
88 review] performed well when integrated over long time  
89 periods (>200 days) but failed to resolve episodic production  
90 events on the order of days to months [Siegel et al., 2001].  
91 Failures in these satellite approaches on regional scales are  
92 probably related to the degree to which particular algorithms  
93 are “tuned” to a specific region and the resolution of the  
94 time step in which satellites sample regions because of  
95 orbital trajectories and the occurrence of cloudy weather.  
96 Ondrusek et al. [2001] also reported that satellite-based  
97 depth-integrated models also did not perform well; how-  
98 ever, estimates were improved using a wavelength-resolved  
99 model. This model was dependent on chlorophyll specific  
100 mean spectrally weighted absorption of phytoplankton ( $\bar{a}_{ph}^*$ ),  
101 which explained 82% of the variance and was able to resolve  
102 small-timescale phytoplankton blooms. Productivity models  
103 that incorporate  $\bar{a}_{ph}^*$  performed well in many different waters  
104 [Smith et al., 1989; Bidigare et al., 1992; Waters et al., 1994;  
105 Morel et al., 1996] because they describe the fraction of  
106 photosynthetically available radiation (PAR) that is  
107 absorbed, which is a function of phytoplankton abundance,  
108 distribution, community structure, and physiology. Most  
109 often studies using these models use chemical extraction  
110 [Kishino et al., 1985] or high-performance liquid chroma-  
111 tography (HPLC) to measure  $\bar{a}_{ph}^*$ , which limits the amount of  
112 data that is available thus making comparisons to satellite  
113 data difficult [Siegel et al., 2001]. Secondly, the presence  
114 of other compounds that absorb light in coastal waters can  
115 complicate these approaches.

116 [5] Between the depth-integrated productivity models and  
117 the laboratory-dependent wavelength-resolved models there  
118 exists a gap in our ability to resolve and assess the episodic  
119 productivity events such as upwelling and river plumes in  
120 coastal systems that potentially account for a significant  
121 portion of the seasonal productivity signal [Walsh, 1978].  
122 Depth-integrated approaches are limited not only in algo-  
123 rithm development but also in the resolution of temporal  
124 coverage due to clouds, while the use of wavelength-  
125 resolved models derived from discrete water samples are  
126 limited to relatively short space and timescales because of  
127 sampling logistics. While there is progress being made in

128 developing satellite productivity algorithms for coastal  
129 turbid waters, the issues of cloud cover persist. Therefore  
130 if we are to understand the episodic nature of coastal systems  
131 on seasonal scales, there is a need to collect parameters for  
132 wavelength-resolved models on high-resolution space and  
133 timescales over broad regions to improve productivity esti-  
134 mates in turbid coastal regions.

135 [6] Here we present a high-resolution time series of in-  
136 water physical and optical data collected by two cabled  
137 profilers as part of the Long-term Ecosystem Observatory  
138 (LEO) [see Schofield et al., 2002] to demonstrate an  
139 approach which can potentially “fill the gap” between  
140 satellite-based depth-integrated productivity models and  
141 productivity models dependent on discrete water samples  
142 such as wavelength-resolved models. From this time series  
143 we directly derive the spectral absorption of phytoplankton  
144 in coastal waters from bulk optical parameters measured  
145 with “off the shelf” technology and quantify its utility in  
146 bio-optically estimating primary productivity in coastal  
147 waters. We discuss assumptions and errors associated with  
148 our approach. These absorption-based bio-optical model  
149 estimates compared well with a physiology-based model  
150 rooted in measured photosynthetic-irradiance ( $P-E$ ) param-  
151 eters. This technique represents a high-resolution approach  
152 to calculating spectrally weighted phytoplankton absorption  
153 independent of laboratory extractions. While the scope of  
154 our study does not and cannot address the scope of the  
155 variability in primary production in the coastal ocean, we  
156 feel that automated optical approaches such as the one  
157 presented here provide a link for wavelength-resolved  
158 models to be applied on broad spatial scales through the  
159 use of autonomous platforms.

## 2. Methods 160

161 [7] The 2000 Hyperspectral Coupled Ocean Dynamics  
162 Experiment (HyCODE) conducted at LEO represents an  
163 integrated coastal-ocean-observing network [Glenn et al.,  
164 2000; Schofield et al., 2002]. As part of this experiment, in-  
165 water physical and bio-optical time series data were col-  
166 lected from two profiling instrument nodes linked to shore  
167 via an electrooptical cable. These nodes were deployed  
168 approximately 4 km offshore in 13 m of water at  
169 39°27.41'N, 74°14.75'W (node B and the optical profiler,  
170 Figure 1). This study represents data collected from calen-  
171 dar days 202-215. Node B provided hydrographic data, and  
172 the optical profiler provided optical data. These nodes were  
173 separated by about 100 m.

### 2.1. Profiler Data Sets 174

175 [8] As opposed to traditional methods of water-column  
176 profiling using lowered instrument packages from ships,  
177 both the optical profiler and node B had frames anchored to  
178 the seafloor with instrument packages attached to floating  
179 drogues that were depth controlled by an underwater winch.  
180 Data measured by these profilers streamed directly to the  
181 Rutgers University Marine Field Station (RUMFS) in real  
182 time via an electrooptical cable, where it was processed  
183 and visualized. Node B included a Sea-Bird conductivity-  
184 temperature-depth (CTD) mounted with a WET Labs  
185 chlorophyll fluorometer, which was sampled at 2 Hz and  
186 was profiled at a vertical rate of 2 cm s<sup>-1</sup> at regular

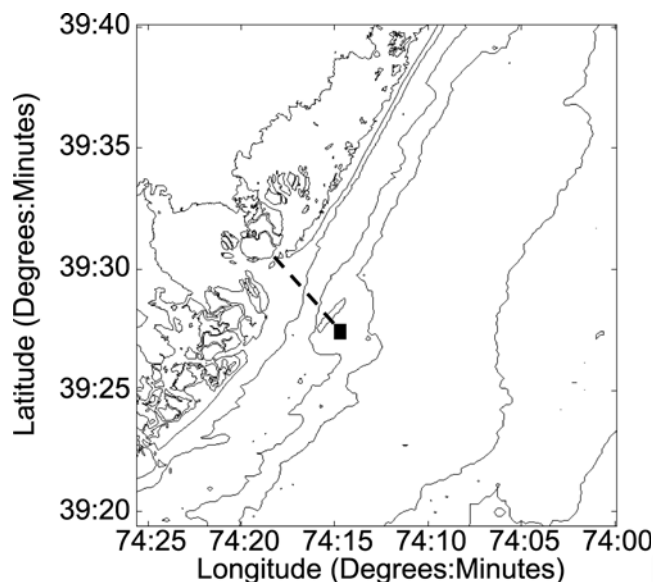


**Figure 1.** Location of node B and optical profiler connected via electrooptical cable (dashed line) to the Rutgers Marine Field Station located in the Mullica River estuary. Bottom contours are the 5-m isobaths.

187 intervals. The optical profiler included a WET Labs nine-  
 188 wavelength absorption/attenuation meter (ac-9) (412, 440,  
 189 488, 510, 532, 555, 650, 676, and 715 nm), which sampled  
 190 at 8 Hz, and a two-wavelength backscatter/fluorometer  
 191 HOBI Labs HydroScat-2 (470 and 676 nm) that sampled  
 192 at 2 Hz. The optical profiler also profiled at a rate of  
 193  $2 \text{ cm s}^{-1}$ . The ac-9 was factory and clean-water calibrated  
 194 prior to the experiment, and absorption values were corrected  
 195 for scattering by subtracting absorption at 715 nm. Absorp-  
 196 tion, attenuation, backscatter, and chlorophyll fluorescence  
 197 data were averaged into 0.25-m bins. Because of the abun-  
 198 dance of gelatinous zooplankton in the water column and  
 199 their impact on the data when in the ac-9 tubes, a data filter  
 200 was applied to eliminate spikes of data of greater than  
 201 300% change in signal for any 0.25-m bin. While this  
 202 would eliminate the potential to document any microlayer  
 203 [Dekshenieks *et al.*, 2001], we believe that the highly  
 204 turbulent nature of these waters would minimize their pres-  
 205 ence. These “spikes” were rare and represented less than 2%  
 206 of the total data. Additionally, discrete measurements at the  
 207 profiler were taken by ship over a series of days at the  
 208 profilers and analyzed for chlorophyll concentration using  
 209 high-performance liquid chromatography to validate the  
 210 fluorometer measurements. Node B logged a total of 255  
 211 downward profiles while 565 downward profiles were  
 212 logged from the optical profiler during this experiment. Both  
 213 node B and optical profiler profiling times were evenly  
 214 distributed over the course of the experiment, with two  
 215 exceptions when node B required servicing for about 4 hours.  
 216 [9] Absorption, attenuation, and backscatter data were  
 217 used as input into a radiative transfer model (Hydrolight  
 218 v. 4.2) to model the spectral scalar irradiance from 400 to  
 219 700 nm. Hydrolight model runs applied [Pope and Fry,  
 220 1997] pure water absorption values. The Hydrolight model  
 221 computed a new spectral scattering phase function when the  
 222 backscatter to total scatter ratio changed by more than

0.005. These model runs also incorporated wind velocity 223  
 measurements from the RUMFS meteorological tower to 224  
 estimate surface roughness. The sky spectral radiance 225  
 distribution is calculated within Hydrolight via RADTRAN 226  
 based on user-supplied date, time, location, and cloud cover. 227  
 This modeled spectral irradiance was scaled to wavelength- 228  
 integrated photosynthetically active radiation values mea- 229  
 sured at the RUMFS field station. The derived spectral 230  
 diffuse attenuation coefficients from Hydrolight were then 231  
 used to propagate the scaled spectral irradiance to all depths. 232

## 2.2. Optical Inversion Model and Mean Spectral 233 Phytoplankton Absorption 234

[10] Binned absorption data collected by the ac-9 were 235  
 inverted using the optical signature inversion (OSI) model 236  
 (O. Schofield *et al.*, Inverting inherent optical signatures in 237  
 the nearshore coastal waters at the Long Term Ecosystem 238  
 Observatory, *Journal of Geophysical Research*, 2003, here- 239  
 inafter referred to as Schofield *et al.*, submitted manuscript, 240  
 2003) to estimate the relative abundance weights of phyto- 241  
 plankton, colored dissolved organic matter (CDOM), and 242  
 detritus. This was based on inverting the bulk ac-9 absorp- 243  
 tion using a series of spectral absorption curves that 244  
 represent the major absorbing constituents in the water 245  
 column. Phytoplankton curves represented the means of 246  
 high-light- and low-light-adapted phytoplankton from three 247  
 major phytoplankton taxa: chlorophyll<sub>a-c</sub>, chlorophyll<sub>a-b</sub>, 248  
 and phycobilin-containing phytoplankton [Johnsen *et al.*, 249  
 1994]. CDOM and detritus absorption curves were treated 250  
 as idealized exponential functions with a variable amplitude 251  
 and spectral exponential decay slope (Figure 2). The OSI 252  
 model varied the amplitudes of all these curves, as well as 253  
 the exponential slopes of the CDOM and detritus curves 254  
 within the boundaries of known constraints to minimize the 255

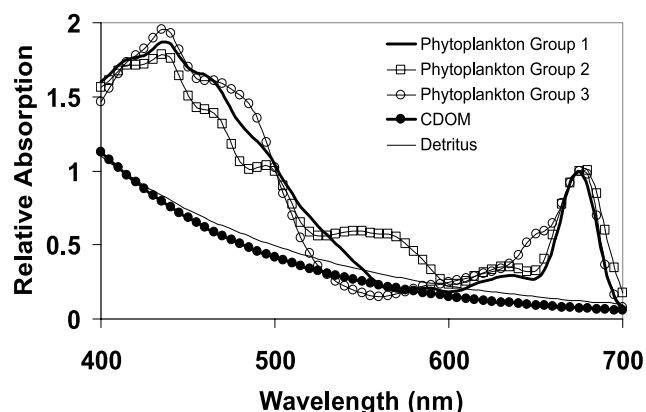


**Figure 2.** Input spectra used to invert the in situ 256  
 absorption values measured by the ac-9 using the OSI 257  
 model. Phytoplankton spectra are averages of high-light- 258  
 and low-light-adapted phytoplankton from Johnsen *et al.* 259  
 [1994]. Phytoplankton group one represents chlorophyll<sub>a-c</sub> 260  
 containing classes of Bacillariophyceae, Dinophyceae, and 261  
 Prymnesiophyceae. Phytoplankton group 2 represents the 262  
 phycobilin-containing class Cryptophyceae. Phytoplankton 263  
 group 3 represents the chlorophyll<sub>a-b</sub> containing classes of 264  
 Chlorophyceae, Prasinophyceae, and Euglenophyceae. 265  
 CDOM and detritus spectra are idealized exponential 266  
 functions.

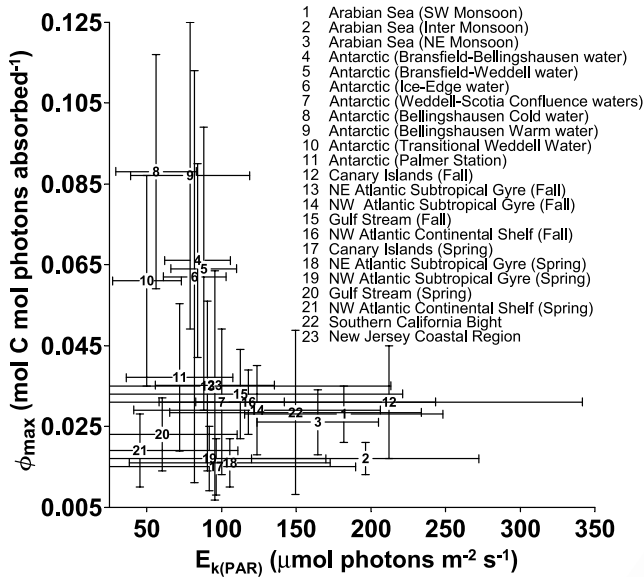


**Figure 3.** Paired  $E_{k(\text{PAR})}$  and  $\phi_{\text{max}}$  reported water column means and standard deviations from various studies: 1–3, *Sathyendranath et al.* [1999]; 4–7, *Figueiras et al.* [1999]; 8–10, *Lorenzo et al.* [2002]; 11, *Moline and Prézélin* [1996]; 13–21, *Kyewalyanga et al.* [1998]; 22, *Schofield et al.* [1993]; and 23 New Jersey Coastal Region (LEO). Antarctic studies are characterized by low  $E_{k(\text{PAR})}$  and high  $\phi_{\text{max}}$ , while the opposite trend is evident for tropical and temperate waters. The mean values for this study for  $E_{k(\text{PAR})}$  and  $\phi_{\text{max}}$  were calculated from all the literature studies in temperate and tropical waters except those estimated at the study site using  $^{14}\text{C}$  incubations (all values not labeled “Antarctic” or “New Jersey Coastal Region (LEO)”).

256 difference between the total modeled absorption (sum of all  
257 phytoplankton, CDOM, and detritus curves) and total absorp-  
258 tion measured by the ac-9. The OSI model returns the  
259 estimated weights of each phytoplankton group, and CDOM  
260 and detritus, as well as the spectral exponential slopes (or  
261 decay) of CDOM and detritus. These weights are analogous  
262 to the amplitude or abundance of their respective absorbing  
263 constituent.

264 [11] Spectral absorption of phytoplankton ( $a_{\text{ph}}(\lambda, z, t)$ )  
265  $\text{m}^{-1}$ ) was calculated by

$$a_{\text{ph}}(\lambda, z, t) = \sum_{n=1}^3 w_{n(\text{ph})}(z, t) a_{n(\text{ph})}(\lambda), \quad (1)$$

267 where  $n$  is the phytoplankton group number,  $w_{n(\text{ph})}(z, t)$  is  
268 the calibrated inverted scalar weight calculated by the OSI  
269 model of a specific group of phytoplankton ( $\text{m}^{-1}$ ), which is  
270 not spectrally dependent, and  $a_{n(\text{ph})}(\lambda)$  is the relative  
271 absorption of the input spectra of specific group of  
272 phytoplankton at a given wavelength. OSI calibration data  
273 showed that the amplitude of the phytoplankton spectra was  
274 generally underestimated due to the package effect of  
275 natural populations compared to the laboratory cultures  
276 from which the input spectra are derived. Although there  
277 was an underestimation, this underestimation was well  
278 quantified so that a calibration factor of 1.393 was applied

to the relative weights of phytoplankton derived by the OSI  
(Schofield et al., submitted manuscript, 2003). Modeled  
spectral scalar irradiance values were combined with  $a_{\text{ph}}(\lambda,$   
 $z, t)$  to calculate the mean spectral absorption of  
phytoplankton  $\bar{a}_{\text{ph}}(\lambda, z, t)$  ( $\text{m}^{-1}$ ) using:

$$\bar{a}_{\text{ph}}(z, t) = \frac{\int_{400}^{700} E_o(\lambda, z, t) a_{\text{ph}}(\lambda, z, t) d\lambda}{\int_{400}^{700} E_o(\lambda, z, t) d\lambda}, \quad (2)$$

where  $E_o(\lambda, z, t)$  is spectral scalar irradiance from 400 to  
700 nm ( $\text{W m}^{-2}$ ) modeled by Hydrolight v. 4.2.

### 2.3. Bio-Optical Modeling of Primary Production From an ac-9

[12] The bio-optical model used in this study to calculate  
primary production was

$$\text{PP}(z, t) = \bar{a}_{\text{ph}}(z, t) \phi_{\text{max}} E_{k(\text{PAR})} \tanh\left(\frac{E_{o(\text{PAR})}(z, t)}{E_{k(\text{PAR})}}\right), \quad (3)$$

where  $\text{PP}(z, t)$  is primary production ( $\text{mg C m}^{-3} \text{h}^{-1}$ ),  $\bar{a}_{\text{ph}}$   
 $(z, t)$  is calculated from equation (2) and was based solely on  
the optical inversion of ac-9 data,  $\phi_{\text{max}}$  is the maximum  
quantum yield of carbon fixation ( $\text{mol C mol photons}$   
absorbed $^{-1}$ ),  $E_{k(\text{PAR})}$  is the irradiant flux at which photo-  
synthesis becomes light saturated ( $\mu\text{mol photons m}^{-2} \text{s}^{-1}$ ),  
and  $E_{o(\text{PAR})}(z, t)$  is the PAR-integrated scalar irradiant flux  
incident on the phytoplankton cells ( $\mu\text{mol photons m}^{-2} \text{s}^{-1}$ )  
modeled by Hydrolight v. 4.2.  $E_{o(\text{PAR})}(z, t)$  was used for this  
calculation because phytoplankton absorbs light from all  
directions. Because our in situ optical data set did not  
include measurements of  $\phi_{\text{max}}$  and  $E_{k(\text{PAR})}$ , we conducted a  
literature survey to determine a mean for these waters  
(Figure 3, see figure legend for references). The data in  
Figure 3 represent the mean and standard deviation of the  
water column measured in each study. The mean  $\phi_{\text{max}}$  and  
 $E_{k(\text{PAR})}$  value used in this study were calculated from all the  
literature studies in temperate and tropical waters except  
from those labeled “Antarctic” or “New Jersey Coastal  
Region (LEO)” in Figure 3. We did not include values of  
 $\phi_{\text{max}}$  and  $E_{k(\text{PAR})}$  estimated by  $^{14}\text{C}$  incubations from the  
LEO site in this mean because we wished to keep the bio-  
optical method of estimating primary productivity and the  
physiological method of estimating productivity as inde-  
pendent as possible. The mean values used for  $\phi_{\text{max}}$  and  
 $E_{k(\text{PAR})}$  for this study were  $0.025 \text{ mol C mol photons}$   
absorbed $^{-1}$  and  $124.85 \mu\text{mol photons m}^{-2} \text{s}^{-1}$ , respectively.  
In this manuscript, this productivity model will be simply  
referred to as the bio-optical model.

### 2.4. Productivity Measurements of Phytoplankton

[13] Discrete water samples were collected at the profilers  
with Niskin bottles from the R/V *Walford* on calendar days  
203, 208, and 212 at both the surface and at a depth of 8 m  
(Table 1). These days coincided with major changes in  
water-column structure that were observed from real-time  
observation of profiler data, which allowed for adaptive  
sampling. These samples were collected at approximately  
1000 LT on these days and kept dark for 30 min while

t1.1 **Table 1.** Phytoplankton Physiological Parameters Measured  
During Experiment

t1.2	Day (Depth)	$P_{\max}$ , mol C m <sup>-3</sup> h <sup>-1</sup>	$E_{k(\text{PAR})}$ , $\mu\text{mol photons m}^{-2} \text{ s}^{-1}$
t1.3	203 (surface)	1.21	146.44
t1.4	203 (8 m)	1.07	55.66
t1.5	208 (surface)	1.38	62.08
t1.6	208 (8 m)	3.05	140.88
t1.7	212 (surface)	1.76	96.09
t1.8	212 (8 m)	3.64	71.23

330 returning to the field station. Aliquots were then filtered  
331 onto 47-mm GF/F filters and stored in an  $-80^{\circ}\text{C}$  freezer for  
332 phytoplankton pigment determination using HPLC analysis  
333 using the methods of *Wright et al.* [1991]. Photosynthetic-  
334 irradiance curves were measured using the methods of  
335 *Prézelin et al.* [1989]. Measured carbon uptake values for  
336 each of the  $P$ - $E$  curves were curve fitted as a hyperbolic  
337 tangent function using the Simplex method of *Caceci and*  
338 *Cacheris* [1984] to estimate the chlorophyll-specific maxi-  
339 mum photosynthetic rate ( $P_{\max}$ , mol C m<sup>-3</sup> h<sup>-1</sup>), the light-  
340 limited slope of photosynthesis ( $\alpha$ ), and the photosynthetic  
341 light-saturation parameter ( $E_{k(\text{PAR})}$ ). Error estimates were  
342 calculated using the methods of *Zimmerman et al.* [1987].  
343 [14] The general model used in this study to calculate  
344 physiology-based primary production is based on the work  
345 of *Jassby and Platt* [1976]:

$$\text{PP}(z, t) = P_{\max}(z, t) \tanh\left(\frac{E_{o(\text{PAR})}(z, t)}{E_{k(\text{PAR})}(z, t)}\right), \quad (4)$$

347 where PP,  $P_{\max}$ ,  $E_{o(\text{PAR})}$ , and  $E_{k(\text{PAR})}$  are as described  
348 previously. To extrapolate physiological parameters ( $P_{\max}$   
349 and  $E_{k(\text{PAR})}$ ) measured at the profiler over the same depth-  
350 time area that the profilers were deployed (give them similar  
351  $z$  and  $t$  distribution as equation (3)), multivariate cluster  
352 analysis of paired salinity and temperature observations  
353 from node B was used to define statistical boundaries on  
354 water masses. Salinity and temperature values were stan-  
355 dardized by subtracting the mean of the data set and  
356 dividing by the standard deviation of the data set. On the  
357 basis of Euclidian distance, a distance matrix was calculated  
358 for the data set and then hierarchically clustered according  
359 to Ward's linkage [*Ward, 1963*]. The generated similarity  
360 index was used in conjunction with a multivariate analysis  
361 of variance (MANOVA) to define the major groupings of  
362 temperature and salinity observations (i.e., water masses).  
363 Physiological parameters were measured within each of the  
364 statistically distinct water masses except a water mass in the  
365 lower portion of the water column on days 213–215. This  
366 restricted physiology-based depth-integrated productivity  
367 calculations to days 202–212. In the case where a specific  
368 water mass was continuous throughout the depth of the  
369 water column, the water mass was subdivided at the 8-m  
370 mark, below the climatological depth of the thermocline in  
371 this area (7 m), so that the physiological parameters mea-  
372 sured at the surface and at 8-m depth in the water mass were  
373 separated. On the basis of this extrapolation method, the  
374 depth-integrated productivity was calculated.

375 [15] The assumptions of this approach do not incorporate  
376 diel variation of physiological parameters, which have been  
377 shown to be important in calculating short-timescale pro-

ductivity [*Sournia, 1974; Prézelin et al., 1987; Prézelin,* 378  
1991]. To mediate these effects, measurements were made 379  
at approximately the same time of day. However, these diel 380  
cycles introduce errors into our comparison of physiology- 381  
based and bio-optical calculations of primary production, 382  
although not just our errors. In this manuscript, this pro- 383  
ductivity model will be referred to as the physiology-based 384  
model. 385

### 3. Results 387

#### 3.1. Hydrographic and Optical Variability at the LEO 388 Profilers 389

[16] The winds, surface currents, and hydrographic struc- 390  
ture of the water column were highly variable with several 391  
major events occurring during the experiment (Figures 4 392  
and 5). These events directly impacted the distribution of 393  
phytoplankton biomass and other absorbing constituents 394  
such as CDOM and detritus that modulate the in-water 395  
spectral light field, therefore affecting what phytoplankton 396  
can absorb for photosynthesis. On calendar days 202–203, 397  
strong northeasterly winds were in phase with the surface 398  
currents, measured using a SeaSonde Radar system, show- 399  
ing a strong southward alongshore flow (Figure 4). The 400  
density structure was stratified during this time period 401  
(Figure 5a). On days 203–205, the winds shift abruptly, 402  
blowing from the southwest, and surface currents progres- 403  
sively rotated toward the northeast. This is coincident with 404  
the appearance of comparatively denser water at the bottom, 405  
which resulted in strong stratification. The presence of this 406  
cold bottom water was reflected in the optical properties. 407  
Associated with the bottom water were smaller particles as 408  
indicated by the backscatter to total scatter ratio (Figure 5b) 409  
[*Stramski and Morel, 1990*]. During these times of strong 410  
stratification the majority of the phytoplankton biomass was 411  
present in the upper water column (Figures 5c and 5d). The 412  
exponential slopes and relative abundance of the CDOM 413  
and detritus also reflected the physical hydrography with 414  
low concentrations and large exponential slopes associated 415  
with the dense bottom water (Figure 6 and Table 2). Large 416

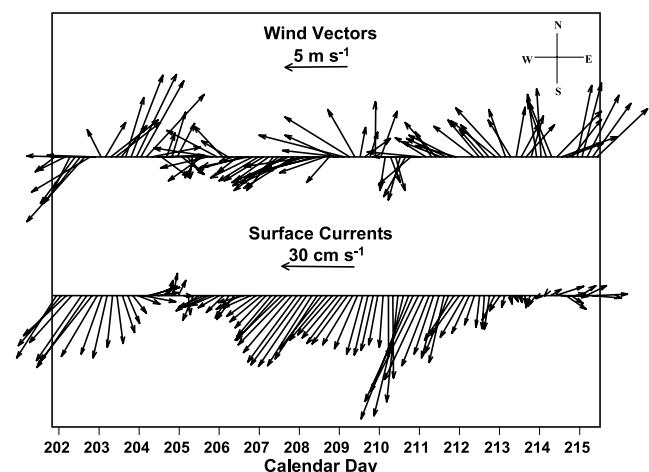


**Figure 4.** Three-hour-averaged wind velocities measured at RUMFS and surface currents measured over the profilers during their deployment. Surface currents are detided and loss-pass filtered. Vector speed is indicated by length.

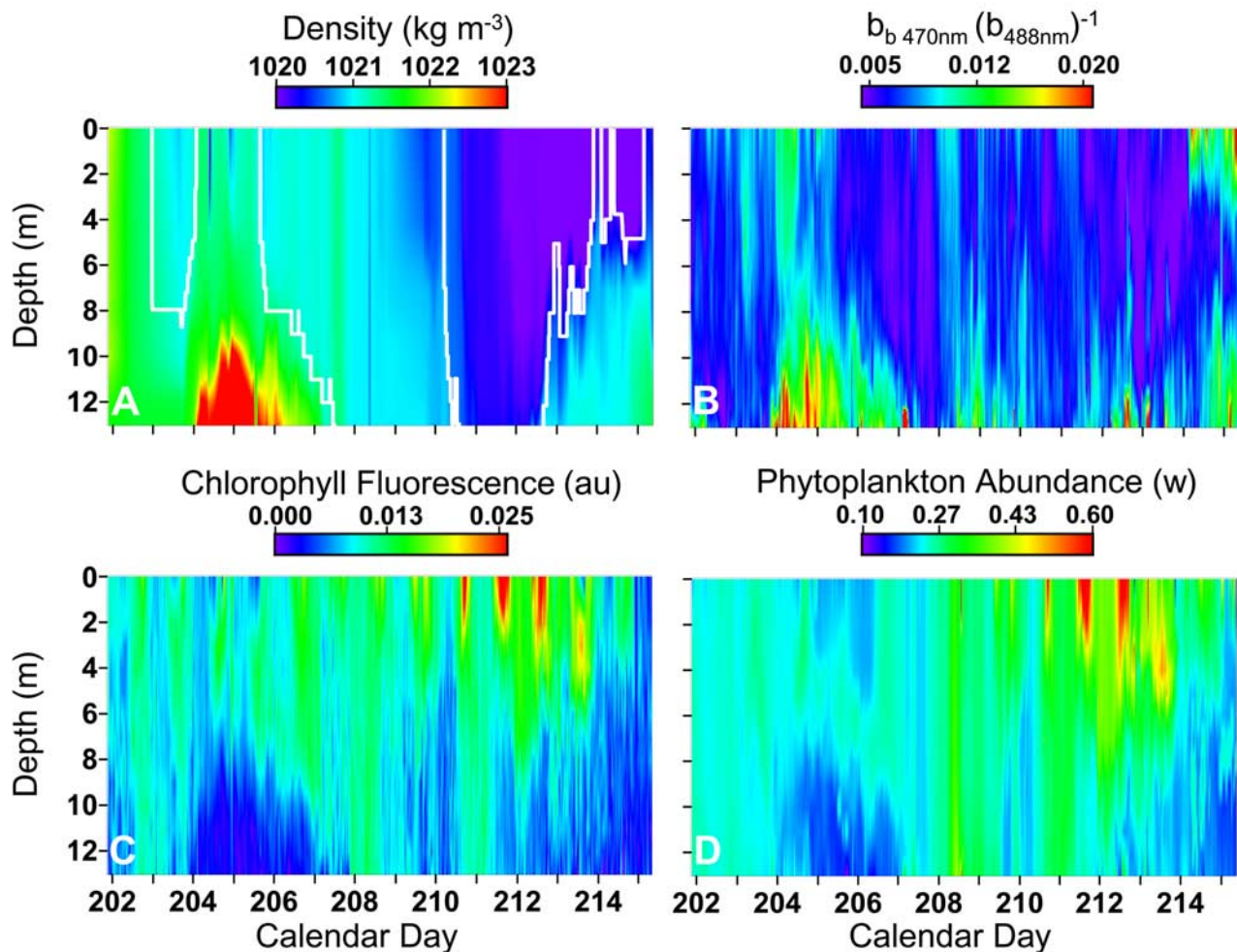


**Figure 5.** Time series of in situ data taken by the profilers during the experiment. (a) Density structure with water mass boundaries (white) defined by cluster analysis (see text). (b) The ratio of scattered and backward scattered light. (c) Chlorophyll fluorescence measured by the optical profiler. (d) The OSI-derived calibrated relative phytoplankton abundance. Optical and biological parameters have similar patterns as the hydrographic structure. Relationships between these bulk optical and derived optical parameters and the density structure are found in Table 2.

417 exponential slopes are often associated with marine-derived  
 418 waters in this region, reflecting the degradation and break-  
 419 ing of double bonds of the CDOM [Vodacek *et al.*, 1997].  
 420 [17] On day 206, winds became northeasterly, and the  
 421 surface currents turned to the southwest; however, the  
 422 bottom water intrusion of dense seawater persisted until  
 423 day 207 when it was eventually dissipated during a period  
 424 of strong winds and increasing current velocities. When the  
 425 stratification eroded, phytoplankton concentrations in-  
 426 creased throughout the water column (Figures 5c and 5d).  
 427 Interestingly, the concentration of the CDOM and detritus  
 428 decreased dramatically throughout the water column during  
 429 these mixing events (Figures 6a and 6c). The northeasterly  
 430 winds persisted until approximately day 208. Despite this,  
 431 surface currents continued to flow southward with increas-  
 432 ing velocity. This trend continued until day 210, when  
 433 winds were from the north, and surface currents were  
 434 flowing  $>60\text{ cm s}^{-1}$  to the south. The entire water column  
 435 during this time was well mixed, with decreased density and  
 436 salinities as low as 28.5 practical salinity unit (Figure 5a).

[18] Cross-shore transects of salinity and temperature to 437  
 the north of the profiler and measured currents surface 438  
 current radars (Figure 4) indicated a large volume of 439  
 southward flowing low-salinity water. Given the large 440  
 volume of relatively fresh water at the profilers, the water 441  
 was likely from the Hudson River [Johnson *et al.*, 2003; 442  
 R. J. Chant and S. M. Glenn, Secondary circulation and 443  
 mixing in a buoyant coastal current, submitted to *Journal of* 444  
*Geophysical Research*, 2003, hereinafter referred to as 445  
 Chant and Glenn, submitted manuscript, 2003]. The pres- 446  
 ence of the Hudson River water was clearly delineated in 447  
 the optical properties reflecting high concentrations of large 448  
 particles (Figure 5b), phytoplankton (Figures 5c and 5d), 449  
 CDOM, and detritus (Figures 6a and 6c). The phytoplank- 450  
 ton community during this experiment was primarily diatom 451  
 based determined by the abundance of fucoxanthin in the 452  
 HPLC samples. Concurrent with the high concentrations of 453  
 CDOM and detritus was a decrease in their respective 454  
 spectral exponential slopes. Low exponential slopes often 455  
 indicate that the CDOM and detrital material are young. 456

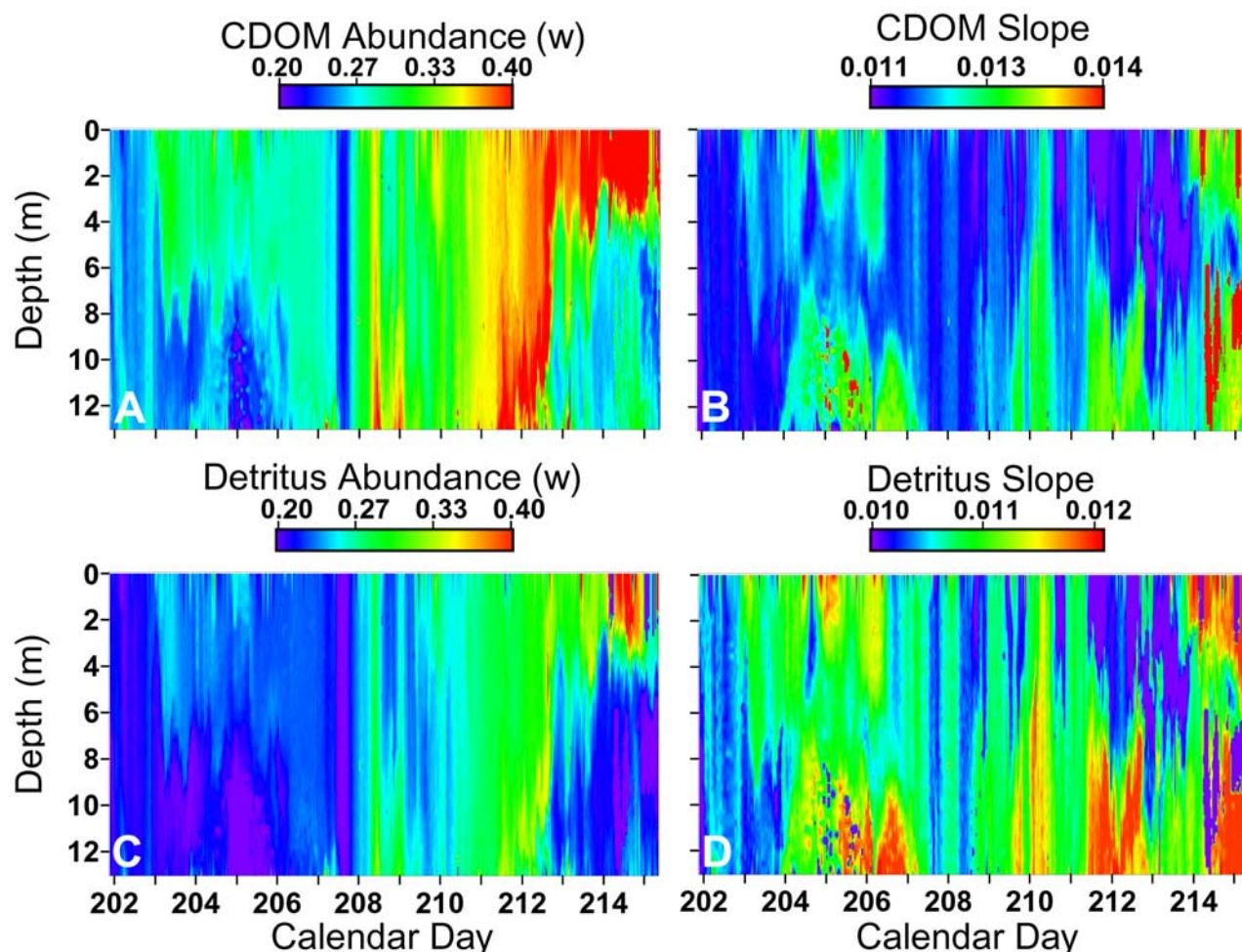


**Figure 6.** Time series of inverted in situ absorption data taken by the optical profiler during the experiment. (a) The relative abundance of CDOM and (b) the exponential slope of the CDOM curve. (c) The relative abundance of detritus and (d) the exponential slope of the detritus curve. Derived optical properties show distinct characteristics of the hydrographic structure during the experiment. Relationships between these derived optical parameters and the density structure are found in Table 2.

457 Local winds did not heavily influence the plume (Chant and  
 458 Glenn, submitted manuscript, 2003) suggesting southward  
 459 flow resulted from a buoyancy-derived pressure gradient.  
 460 Alternating southeast and southwest winds blew from days  
 461 211 to 215 while the surface currents weakened and  
 462 eventually the currents veered offshore (Figure 4). Associ-  
 463 ated with this was a restratification and intrusion of dense  
 464 bottom waters. As before, the dense bottom waters were  
 465 characterized by low concentrations of phytoplankton,  
 466 CDOM, detritus, and small particles (Figures 5 and 6).

467 [19] The clustering scheme applied to the hydrographic  
 468 data suggests that at least three water masses were advected  
 469 past and sampled by the profilers. A MANOVA showed that  
 470 the three water masses defined by this clustering scheme  
 471 were significantly different (Pillai Trace approximately  $F =$   
 472  $2988.747$ ,  $p = 0.000$ ). The major features defined by cluster  
 473 analysis as specific water mass types were the deep intru-  
 474 sions on calendar days 202–207 and 212–215, intermediate  
 475 mixed regime on calendar days 206–210, and the Hudson  
 476 River Plume on calendar days 210–214 (Figure 5a). This  
 477 clustering was also consistent with the major changes  
 478 observed in the in situ optical properties and derived optical

constituents (Figures 5 and 6). While the time series shown 479  
 has multiple forcing events, in general, as the water column 480  
 becomes less dense, absorption and attenuation increased as 481  
 well as the derived loads of phytoplankton biomass, 482  
 CDOM, and detritus. This suggests that the high optical 483  
 loads during this time period may be terrestrial in origin. 484

**Table 2.** Correlation of Inherent and Derived Optical Properties  
 With Density<sup>a</sup> t2.1

Variable	$R^2$	Slope	t2.2
$A_{(488)}$ , $m^{-1}$	0.58	–	t2.3
$C_{(488)}$ , $m^{-1}$	0.27	–	t2.4
$B_{p(470)}$ , $m^{-1}$	0.06	+	t2.5
$B_{p(470)}/B_{(488)}$	0.27	+	t2.6
Chlorophyll fluorescence	0.22	–	t2.7
$W_{(phyto)}$	0.46	–	t2.8
$W_{(CDOM)}$	0.59	–	t2.9
$W_{(detritus)}$	0.60	–	t2.10
$S_{(CDOM)}$	0.03	+	t2.11
$S_{(detritus)}$	0.02	+	t2.12

<sup>a</sup>Although not all correlations are strong, they are significant ( $p = 0.000$ ).  
 In general, high optical loads are associated with less dense water. This  
 suggests that optical loads during this time period are terrestrial in nature. t2.13

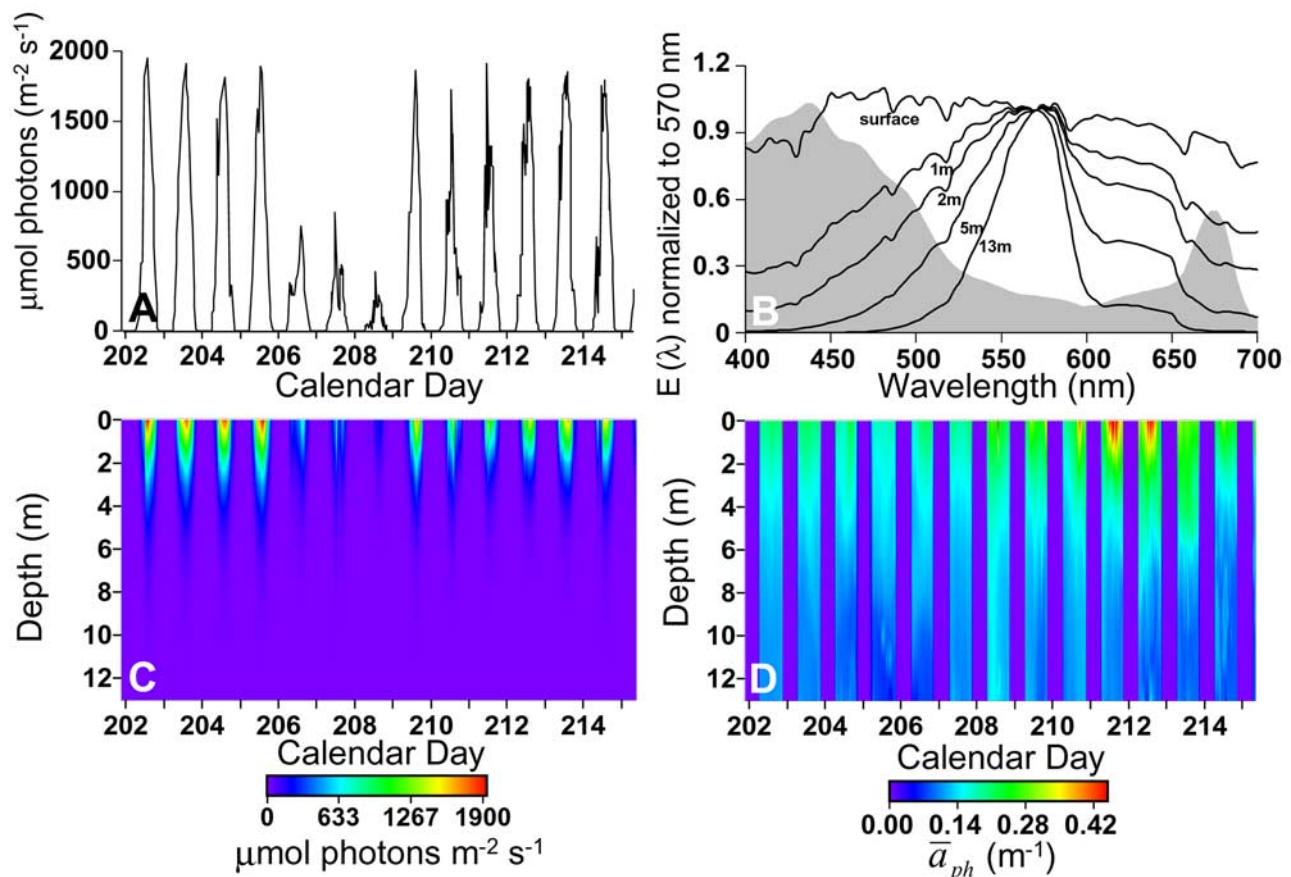


**Figure 7.** (a) The time series of incident  $E_{d(\text{PAR})}$  at the profilers. Noontime values of  $E_{k(\text{PAR})}$  varied by a factor of 4 because of passing storms. (b) A representative normalized profile of  $E_{d(\lambda)}$  at the surface and  $E_o(\lambda)$  at specific depths (solid lines) compared to the mean spectral shape of phytoplankton groups 1, 2, and 3. (c) The propagation of  $E_{o(\text{PAR})}$  through the water column.  $E_{o(\text{PAR})}$  values attenuated quickly because of the turbid nature of the region. The rapid attenuation of the blue wavelengths by CDOM and detritus and red wavelengths by water illustrate the mechanism for modulating  $\bar{a}_{\text{ph}}$  with depth. (d) The distribution of  $\bar{a}_{\text{ph}}$  during the experiment. Large values are coincident with the largest biomass signal. Nighttime profiles were assumed to be zero.

485 Conversely, the particle size index (ratio of backscatter to  
486 total scatter), and the spectral exponential slopes of CDOM  
487 and detritus were positively correlated. This suggests that  
488 steeper slopes and smaller particles are coincident with  
489 marine waters during this time period (Table 2).

### 490 3.2. Spectrally Weighted Phytoplankton Absorption

491 [20] Surface irradiance during the course of the experi-  
492 ment was highly variable due to passing storms and patchy  
493 cloud cover. Peak  $E_{d(\text{PAR})}$  values during the clearest atmo-  
494 spheric days approached  $2000 \mu\text{mol photons m}^{-2} \text{s}^{-1}$  while  
495 surface irradiance values during stormy days were four  
496 times lower (Figure 7a). In general, PAR attenuated rapidly,  
497 with its first attenuation length usually 0.5–1.5 m deep  
498 (Figure 7c). Modeled hyperspectral profiles of  $E_o(\lambda)$  indi-  
499 cated that attenuation was largest in the wavelengths asso-  
500 ciated with maximal absorption peaks of chlorophyll,  
501 illustrating the importance of phytoplankton to bulk optical  
502 properties. Similar to chlorophyll biomass, values of  $\bar{a}_{\text{ph}}$   
503 calculated from equation (2) showed the largest values in  
504 the Hudson River water mass and the lowest values in the  
505 deep water intrusions. However,  $\bar{a}_{\text{ph}}$  decreased and smeared

506 with depth due to the decreased availability of red and blue  
507 wavelengths of light at depth. The  $\bar{a}_{\text{ph}}$  thus did not reflect  
508 the same vertical and temporal structure as chlorophyll  
509 fluorescence because the wavelengths at which chlorophyll  
510 absorbs maximally were differentially attenuated more  
511 rapidly in the water column due to the spectral optical  
512 structure of the water column (Figures 7b and 7d).

### 513 3.3. Physiology and ac-9-Derived Bio-Optically Based 514 Primary Production

515 [21] To extrapolate discrete  $^{14}\text{C}$  measurements over time,  
516 measured physiological variables associated with  $^{14}\text{C}$  incu-  
517 bations were assigned to specific water masses defined by  
518 multivariate cluster analysis of temperature and salinity as  
519 described in section 2.4. These physiological measurements  
520 extrapolated into depth and time space using water mass  
521 analysis were then combined with the continuous light fields  
522 based on the in situ optical profiler measurements and the  
523 Hydrolight calculations (Figure 7c). Values were integrated  
524 over depth and will be herein referred to as the productivity  
525 calculated through the physiology-based model. This time  
526 series of depth-integrated primary production was compared

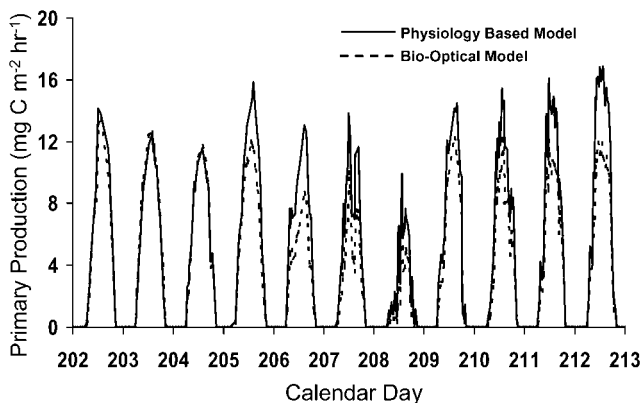


**Figure 8.** Using mean-paired  $E_{k(\text{PAR})}$  and  $\phi_{\text{max}}$  from temperate and tropical oceans excluding this study, bio-optically modeled (dashed) and physiology-based productivity that was extrapolated on the basis of the water mass analysis (solid) was in good agreement across all days ( $r^2 = 0.91$ ,  $p < 0.001$ ). The total productivity predicted by the two models was different by 20%.

527 to the bio-optical model estimates using the ac-9-derived  
528 weighted phytoplankton absorption and equation (3).

529 [22] To convert  $\bar{a}_{\text{ph}}$  into a productivity rate, we required  
530 estimates of  $\phi_{\text{max}}$  and  $E_{k(\text{PAR})}$  which were taken from the  
531 literature (Figure 3). Using the mean values for  $\phi_{\text{max}}$   
532 ( $0.025 \text{ mol C mol photons}^{-1}$ ) and  $E_{k(\text{PAR})}$  ( $124.85 \mu\text{mol}$   
533  $\text{photons m}^{-2} \text{ s}^{-1}$ ) for temperate marine waters, the depth-  
534 integrated bio-optical model showed good agreement with  
535 depth-integrated physiology-based model ( $r^2 = 0.91$ ,  $p <$   
536  $0.001$ ) (Figure 8). Assuming a constant  $\phi_{\text{max}}$  and  $E_{k(\text{PAR})}$   
537 values is known to be problematic, so we conducted a  
538 sensitivity analysis over the range of  $\phi_{\text{max}}$  and  $E_{k(\text{PAR})}$   
539 observed in the world's oceans. The sensitivity analysis is  
540 presented as isoclines in Figure 9. The isoclines represent the  
541 average percent difference between the physiology and bio-  
542 optical-modeled productivity in our study. These differences  
543 were calculated for three timescales, and all showed the

544 general inverse relationship between  $\phi_{\text{max}}$  and  $E_{k(\text{PAR})}$ . The  
545 purpose of time-integrating water-column productivity over  
546 these three scales is that they address the short- to medium-  
547 timescale events which characterize physical forcing and  
548 biological responses in the LEO-15 research area (S. M.  
549 Glenn et al., Studying the biogeochemical impact of sum-  
550 mertime upwelling using a coastal ocean observatory, sub-  
551 mitted to *Journal of Geophysical Research*, 2003, hereinafter  
552 referred to as Glenn et al., submitted manuscript, 2003).  
553 Interestingly, the mean-paired  $\phi_{\text{max}}$  and  $E_{k(\text{PAR})}$  observations  
554 from our literature survey (Figure 3) were generally coincident  
555 with the error minima (Figure 9).

## 4. Discussion

### 4.1. Physical and Optical Properties of the Study Site

559 [23] Southwesterly wind-driven coastal upwelling is an  
560 annual event at LEO and has been observed every summer  
561 over the last decade (Glenn et al., submitted manuscript,  
562 2003). These upwelling-favorable events result in phyto-  
563 plankton blooms [Schofield et al., 2002] and represent one  
564 of the dominant biogeochemical signals in nearshore (<30 m  
565 depth) New Jersey coastal waters (Glenn et al., submitted  
566 manuscript, 2003). However, the optical properties in the  
567 region are complex due to the proximity of the Mullica  
568 River estuary (Figure 1) and the presence of coastally  
569 trapped freshwater plumes from the Hudson River, which  
570 introduce significant amounts of CDOM and detritus.  
571 Therefore the waters at LEO are often classified as “case  
572 2” [Morel and Prieur, 1977]. The  $T$ - $S$  relationships in this  
573 study indicated the presence of significantly different water  
574 masses; however, their boundaries were difficult to resolve  
575 from a  $T$ - $S$  diagram alone. Measured and derived optical  
576 properties were also highly variable and showed significant  
577 correlations to hydrographic structure (Table 2).

### 4.2. Bio-Optical Modeling of Photosynthesis in Coastal Waters

580 [24] Implicit in many primary production models is some  
581 parameterization of  $\bar{a}_{\text{ph}}$  [cf. Bidigare et al., 1992], which has

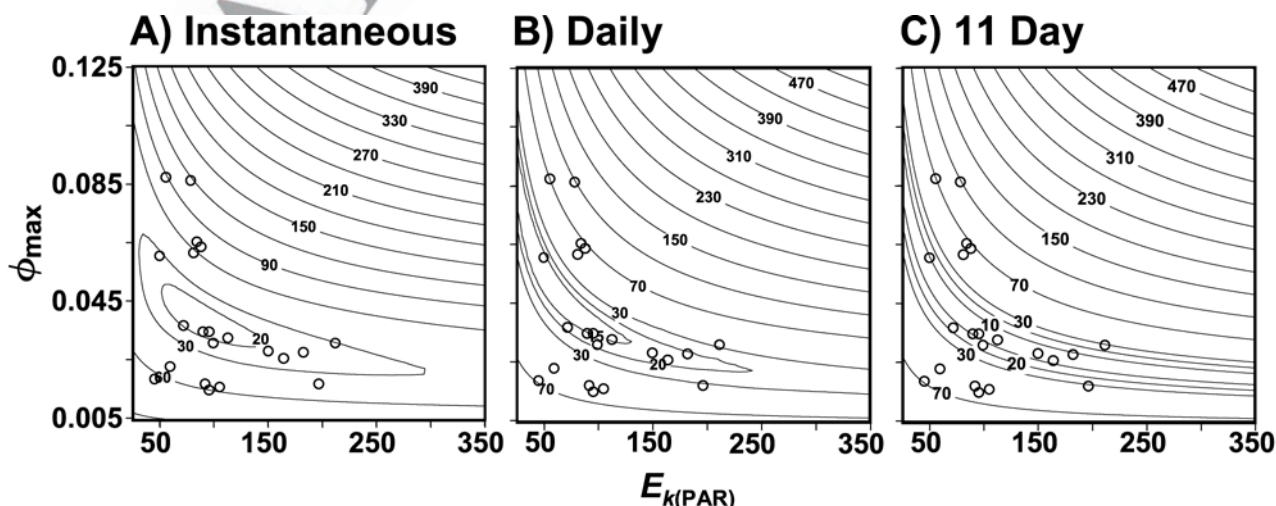


**Figure 9.** (a)–(c) Relative percent error isoclines between the  $^{14}\text{C}$  extrapolated to the ac-9-based water-column-integrated productivity estimates over instantaneous, daily, and 11-day timescales, respectively. The shape of these contours shows the effect of  $\phi_{\text{max}}$  and  $E_{k(\text{PAR})}$  covariance on modeled productivity estimates. Data points represent literature means from Figure 3 and are coincident with the error isoclines.

traditionally been measured using discrete water samples or estimated empirically [Bricaud *et al.*, 1995; Cleveland, 1995]. Often  $\bar{a}_{\text{ph}}$  is derived from the product of biomass and biomass-normalized phytoplankton absorption ( $\bar{a}_{\text{ph}}^*$ ) [Sakshaug *et al.*, 1997]. The utility of this approach is limited given the laboratory requirements for deriving  $\bar{a}_{\text{ph}}^*$ , and the well-documented variability in  $\bar{a}_{\text{ph}}^*$  seasonally [Sathyendranath *et al.*, 1999], regionally [Bricaud and Stramski, 1990; Hoepffner and Sathyendranath, 1992; Sosik, 1996; Arbones *et al.*, 2000], and physiologically [Prézelin and Boczar, 1986; Lewis *et al.*, 1988; Bricaud *et al.*, 1995]. Ideally, the parameterization of  $\bar{a}_{\text{ph}}^*$  is not needed if  $\bar{a}_{\text{ph}}$  could easily be derived from in situ bulk optical measurements. Currently, off-the-shelf technology offers the potential to measure bulk optical properties [Dickey, 1991; Chang and Dickey, 1999].

[25] High-resolution maps of  $\bar{a}_{\text{ph}}$  can be derived from an ac-9 (Figure 7d) allowing wavelength dependency of phytoplankton absorption and spectral light quality to be estimated. To first order  $\bar{a}_{\text{ph}}$  is described by chlorophyll biomass ( $r^2 = 0.71$ ,  $p = 0.000$ ); however,  $\bar{a}_{\text{ph}}$  is a consistently decreasing function with depth. This decrease, a second-order effect, reflects the spectral skewing of light with depth. This spectral skewing of  $\bar{a}_{\text{ph}}$  was sensitive to the relative concentrations of the other in-water constituents. For example, when CDOM and detritus signals were large (day 210) blue wavelengths (400–450 nm) of light were attenuated 30% faster than when CDOM and detritus signals were low (day 202). In contrast, the difference in red wavelength (650–700 nm) attenuation was approximately 7%. The result of this variable skewing of the in situ light field accounts for the scatter between the phytoplankton fluorescence estimates and  $\bar{a}_{\text{ph}}$ . Given in situ  $\bar{a}_{\text{ph}}$  and  $E_{\text{PAR}}$ , the remaining difficulty for estimating photosynthesis is defining the magnitude of  $\phi_{\text{max}}$  and  $E_{k(\text{PAR})}$  as these terms cannot currently be derived optically. While  $\phi_{\text{max}}$  has been related to fluorescence transients via fast repetition rate fluorometry [Kolber *et al.*, 1988; Falkowski, 1992; Kolber and Falkowski, 1993], conversion of the electrons generated by photosystem II to carbon fixation is difficult [Kroon and Dijkman, 1996]. This conversion requires a thorough understanding of the environmental and physiological regulation of the photosynthetic quotient [Laws, 1991]. In nature, both  $\phi_{\text{max}}$  and  $E_{k(\text{PAR})}$  are variable in time and space ranging from hours to seasons [Sournia, 1974; Prézelin, 1991; Kyewalyanga *et al.*, 1998; Gong *et al.*, 1999; Sathyendranath *et al.*, 1999; Marra *et al.*, 2000] and meters to kilometers [Schofield *et al.*, 1993; Lindley *et al.*, 1995; Sosik, 1996; Kyewalyanga *et al.*, 1998]. Over these scales,  $\phi_{\text{max}}$  and  $E_{k(\text{PAR})}$  can vary by a factor of 10 and 5, respectively. To compensate for this effect,  $E_{k(\text{PAR})}$  has been empirically or theoretically parameterized from underwater irradiance fields [Waters *et al.*, 1994; Moline *et al.*, 1998]. Parameterizations of  $\phi_{\text{max}}$  have proven difficult, and so is often assumed to be constant or is measured using radiolabel incubations [Marra, 1993; Waters *et al.*, 1994; Ondrusek *et al.*, 2001]. It was a pleasant surprise then that using temperate and tropical ocean means of  $\phi_{\text{max}}$  and  $E_{k(\text{PAR})}$  from the literature resulted in such a good agreement of physiology-based productivity. Therefore we felt this serendipitous result merited further analysis.

[26] The relationship between  $\bar{a}_{\text{ph}}$ ,  $E_{k(\text{PAR})}$ , and  $\phi_{\text{max}}$  is coupled via

$$E_{k(\text{PAR})} = \frac{P_{\text{max}}}{\phi_{\text{max}} \bar{a}_{\text{ph}}}, \quad (5)$$

which implies a general inverse, covariant relationship between the product of  $\phi_{\text{max}}$  and  $\bar{a}_{\text{ph}}$ , and  $E_{k(\text{PAR})}$ . However, sensitivity analyses of these terms in bio-optical productivity models [Sosik, 1996] suggest that  $\bar{a}_{\text{ph}}$  is not strongly coupled to either  $E_{k(\text{PAR})}$  or  $\phi_{\text{max}}$ . This effect is probably a function of photoprotective pigments [Bidigare *et al.*, 1989; Schofield *et al.*, 1996]. In contrast,  $E_{k(\text{PAR})}$  and  $\phi_{\text{max}}$  appear to be strongly coupled with each other [see Figure 6 in the work of Sosik, 1996]. This is supported by the nonnormal natural distribution of  $\phi_{\text{max}}$  and  $E_{k(\text{PAR})}$  which shows an inverse distribution suggesting that  $\phi_{\text{max}}$  and  $E_{k(\text{PAR})}$  covary in a nonlinear fashion (Figures 3 and 9). This implies that their errors are not additive. Therefore determining the sensitivity of an absorption-based bio-optical model without considering this covariance would overestimate the importance of the variability of  $\phi_{\text{max}}$  and  $E_{k(\text{PAR})}$  to a productivity estimate. Because of this we varied  $\phi_{\text{max}}$  and  $E_{k(\text{PAR})}$  over their natural ranges independent of other water-column properties to quantify their impact on water-column productivity. In addition, this error analysis assumed that errors in the model related to the production of photoprotective pigments were low because they were found in negligible amounts in the HPLC analysis (zeaxanthin 0.1–0.2  $\mu\text{g L}^{-1}$ ) during the experiment and because of the highly turbid nature of the water column.

[27] The net result of this analysis is that the variation in  $\phi_{\text{max}}$  dominates the error in the productivity estimates over hourly, daily, and 11-day timescales in temperate waters (Figure 9). This is not surprising given past field results in which  $\phi_{\text{max}}$  varied by a factor of 10 [Bannister and Weidemann, 1984; Cleveland *et al.*, 1989; Schofield *et al.*, 1993; Babin *et al.*, 1996]. While the bio-optical model was very sensitive to  $\phi_{\text{max}}$ , when considering literature values, the variability in  $\phi_{\text{max}}$  is remarkably constrained temperate and tropical waters ranging from  $\sim 0.015$  to  $0.04$  mol C mol photons absorbed<sup>-1</sup>. Generally, the highest values are found at depth, often near nutriclines [Cleveland *et al.*, 1989], where photosynthesis is light limited. Therefore the impact on integrated water-column productivity is relatively small. In these temperate waters,  $E_{k(\text{PAR})}$  varies by a factor of 7 ( $50$ – $350$   $\mu\text{mol photons m}^{-2} \text{s}^{-1}$ ), reflecting photoacclimation processes [Falkowski and LaRoche, 1991; Escoubas *et al.*, 1995]. However, the impact of  $E_{k(\text{PAR})}$  variability is relatively small in our analysis, as is evidenced by the elongation of the error contours along the  $E_{k(\text{PAR})}$  axis (Figure 9). This reflects that a change in  $E_{k(\text{PAR})}$  (especially when  $E_{k(\text{PAR})} > 100$ ) does not dramatically impact the proportion of the total water-column photosynthesis that is light-saturated as this is largely determined by the exponential decay of light. It is the combined effect of naturally constrained  $\phi_{\text{max}}$  values and the rapid exponential decay of light in our system that allow for our approach of bio-optically estimating productivity to reasonably approximate the physiology-based model.

[28] While these general paradigms apply to temperate and tropical waters, caution should be used, as this is not a global phenomenon. In the Southern Ocean, discrete and

703 water-column-averaged  $\phi_{\max}$  values (Figures 3 and 9) are  
 704 on average two times higher than that measured in tropical  
 705 and temperate waters. The variance in  $\phi_{\max}$  is also high. In  
 706 these polar waters the  $E_{k(\text{PAR})}$  magnitude ( $<100 \mu\text{mol}$   
 707 photons  $\text{m}^{-2} \text{s}^{-1}$ ) and variability (factor of 4) is low. Given  
 708 equation (3) and that mean and variability of  $E_{k(\text{PAR})}$  are  
 709 relatively low, the light-saturated photosynthetic term is  
 710 dominated by the product of  $\phi_{\max}$  and  $\bar{a}_{\text{ph}}$ .

711 [29] In contrast, the tropical and temperate oceans are  
 712 generally stratified much of the year and have high-incident  
 713 irradiance during the phytoplankton growing season. Be-  
 714 cause of these factors, the euphotic zone is generally nutrient  
 715 limited. The combination of low nutrient with high-light  
 716 conditions can reduce the average water column,  $\phi_{\max}$ . This  
 717 decrease reflects the production of photoprotective pigments  
 718 [Bidigare et al., 1989; Schofield et al., 1996; Fujita et al.,  
 719 1994; Babin et al., 1996] and a decrease in functional  
 720 photosynthetic reaction centers [Falkowski et al., 1989].  
 721 The phytoplankton response to the high-light environment  
 722 is an increase in  $E_{k(\text{PAR})}$  given a sufficiently stable environ-  
 723 ment [Ryther and Menzel, 1959; Côté and Platt, 1983].

## 725 5. Conclusions

726 [30] Bio-optical measurements show promise for map-  
 727 ping phytoplankton; however, these techniques have often  
 728 been compromised in turbid coastal waters. The bulk and  
 729 derived optical parameters mimicked the hydrographic  
 730 structure that was dominated by three distinct water masses  
 731 advected through the study area. The correlations of density  
 732 with bulk/derived optical properties suggest that much of  
 733 the optical load is from terrestrial sources. Calculated  $\bar{a}_{\text{ph}}$ ,  
 734 from the relative phytoplankton weight and spectral irradi-  
 735 ance showed that  $\bar{a}_{\text{ph}}$  was to first order a function of  
 736 biomass but was modulated based on the spectral absorbing  
 737 characteristics of in-water biotic and nonbiotic constituents.  
 738 In addition,  $\bar{a}_{\text{ph}}$  could be used to initialize a bio-optical  
 739 productivity model and calculate productivity within 20%  
 740 given reasonable estimates of  $\phi_{\max}$  and  $E_{k(\text{PAR})}$ . Sensitivity  
 741 analysis of the bio-optical model indicated that most of the  
 742 error is potentially associated with  $\phi_{\max}$ ; however, the  
 743 natural range of water-column-averaged  $\phi_{\max}$  is constrained.  
 744 The bio-optical model was not as sensitive to  $E_{k(\text{PAR})}$  when  
 745 estimating water-column productivity because of the expo-  
 746 nential decay of light in these turbid waters.

747 [31] **Acknowledgments.** Special thanks to two anonymous reviewers  
 748 whose comments significantly improved the flow and content of this  
 749 manuscript. Thanks and cold beer owed to Mike Crowley, Josh Kohut,  
 750 Erica Heine, Mike Purcell, Christy Herren, Amanda Ashe, Dwight  
 751 Peterson, Grace Chang, Sage Lichtenwalner, and Alan Weidmann. Support  
 752 was provided by the Office of Naval Research's COMOP and HyCODE  
 753 programs (N00014-97-0767, N0014-99-0196), and the National Ocean  
 754 Partnership Program (N00014-97-1-1019).

## 755 References

756 Arbones, B., F. G. Figueiras, and R. Varela (2000), Action spectrum and  
 757 maximum quantum yield of carbon fixation in natural phytoplankton  
 758 populations: Implications for primary production estimates in the ocean,  
 759 *J. Mar. Syst.*, 26, 97–114.  
 760 Babin, M., A. Morel, H. Claustre, A. Bricaud, Z. Kolber, and P. G. Falkowski  
 761 (1996), Nitrogen- and irradiance-dependent variations of the maximum  
 762 quantum yield of carbon fixation in eutrophic, mesotrophic, and oligo-  
 763 trophic marine systems, *Deep Sea Res., Part I*, 43(8), 1241–1272.  
 764 Bannister, T. T., and A. D. Weidemann (1984), The maximum quantum  
 765 yield of phytoplankton photosynthesis in situ, *J. Plankton Res.*, 6(2),  
 766 275–294.

Behrenfeld, M. J., and P. G. Falkowski (1997), A consumer's guide to 767  
 phytoplankton productivity models, *Limnol. Oceanogr.*, 42(7), 1479– 768  
 1491. 769  
 Bidigare, R. R., O. Schofield, and B. B. Prézelin (1989), Influence of 770  
 zeaxanthin on quantum yield of photosynthesis of *Synechococcus* clone 771  
 WH7803 (DC2), *Mar. Ecol. Prog. Ser.*, 56, 177–188. 772  
 Bidigare, R. R., B. B. Prézelin, and R. C. Smith (1992), Bio-optical models 773  
 and the problems of scaling, in *Primary Productivity and Biogeochemical* 774  
*Cycles in the Sea*, edited by P. G. Falkowski, pp. 175–212, Plenum, New 775  
 York. 776  
 Bienfang, P. K., and D. A. Ziemann (1992), The role of coastal high latitude 777  
 ecosystems in global export production, in *Primary Productivity and* 778  
*Biogeochemical Cycles in the Sea*, edited by P. G. Falkowski, pp. 175– 779  
 212, Plenum, New York. 780  
 Biscaye, P. E., C. N. Flagg, and P. G. Falkowski (1994), The shelf edge 781  
 exchange experiment, Seep, II, An introduction to hypotheses, results and 782  
 conclusions, *Deep Sea Res., Part II*, 41(2), 231–253. 783  
 Bricaud, A., and D. Stramski (1990), Spectral absorption coefficients of 784  
 living phytoplankton and nonalgal biogenous matter: A comparison be- 785  
 tween the Peru upwelling area and the Sargasso Sea, *Limnol. Oceanogr.*, 786  
 35(3), 562–582. 787  
 Bricaud, A., M. Babin, A. Morel, and H. Claustre (1995), Variability in the 788  
 chlorophyll-specific absorption coefficients of natural phytoplankton: 789  
 Analysis and parameterization, *J. Geophys. Res.*, 100(C7), 13,321– 790  
 13,332. 791  
 Brink, K. H. (1997), Observational coastal oceanography, paper presented 792  
 at National Science Foundation, paper presented at OCE Workshops, 793  
 Natl. Sci. Found., Monterey Bay, Calif. 794  
 Cacci, M. S., and W. P. Cacheris (1984), Fitting curves to data, *Byte*, 9, 795  
 340–362. 796  
 Chang, G. C., and T. D. Dickey (1999), Partitioning in situ spectral absorp- 797  
 tion by use of moored spectral absorption-attenuation meters, *Appl. Opt.*, 798  
 38(15), 3876–3887. 799  
 Cleveland, J. S. (1995), Regional models for phytoplankton absorption as a 800  
 function of chlorophyll a concentration, *J. Geophys. Res.*, 100(C7), 801  
 13,333–13,344. 802  
 Cleveland, J. S., M. J. Perry, D. A. Kiefer, and M. C. Talbot (1989), 803  
 Maximal quantum yield of photosynthesis in the northwestern Sargasso 804  
 Sea, *J. Mar. Res.*, 47, 869–886. 805  
 Cloern, J. E. (2001), Our evolving conceptual model of the coastal eutro- 806  
 phication problem, *Mar. Ecol. Prog. Ser.*, 210, 223–253. 807  
 Côté, B., and T. Platt (1983), Day-to-day variations in the spring-summer 808  
 photosynthetic parameters of coastal marine phytoplankton, *Limnol.* 809  
*Oceanogr.*, 28(2), 320–344. 810  
 Dekshenieks, M. M., P. L. Donaghay, J. M. Sullivan, J. E. B. Rines, T. R. 811  
 Osborn, and M. S. Twardowski (2001), Temporal and spatial occurrence 812  
 of thin phytoplankton layers in relation to physical processes, *Mar. Ecol.* 813  
*Prog. Ser.*, 223, 61–71. 814  
 Dickey, T. D. (1991), The emergence of concurrent high-resolution physical 815  
 and bio-optical measurements in the upper ocean and their applications, 816  
*Rev. Geophys.*, 29(3), 383–413. 817  
 Escoubas, J. M., M. Lomas, J. LaRoche, and P. G. Falkowski (1995), Light 818  
 intensity regulation of cab gene transcription is signaled by the redox 819  
 state of the plastoquinone pool, *Proc. Natl. Acad. Sci. U. S. A.*, 92, 820  
 10,237–10,241. 821  
 Falkowski, P. G. (1992), Molecular ecology of phytoplankton photosynthe- 822  
 sis, in *Primary Productivity and Biogeochemical Cycles in the Sea*, 823  
 edited by P. G. Falkowski, pp. 47–67, Plenum, New York. 824  
 Falkowski, P. G., and J. LaRoche (1991), Acclimation to spectral irradiance 825  
 in algae, *J. Phycol.*, 27, 8–14. 826  
 Falkowski, P. G., A. Sukenik, and R. Herzig (1989), Nitrogen limitation in 827  
*Isochrysis galbana* (Haptophyceae), II, Relative abundance of chloroplast 828  
 proteins, *J. Phycol.*, 25, 471–478. 829  
 Falkowski, P. G., P. E. Biscaye, and C. Sancetta (1994), The lateral flux of 830  
 biogenic particles from the eastern North American continental margin to 831  
 the North Atlantic Ocean, *Deep Sea Res., Part II*, 41(2), 583–602. 832  
 Field, C. B., M. J. Behrenfeld, J. T. Randerson, and P. Falkowski (1998), 833  
 Primary production of the biosphere: Integrating terrestrial and oceanic 834  
 components, *Science*, 281, 237–240. 835  
 Figueiras, F. G., B. Arbones, and M. Estrada (1999), Implications of bio- 836  
 optical modeling of phytoplankton photosynthesis in Antarctic waters: 837  
 Further evidence of no light limitation in the Bransfield Strait, *Limnol.* 838  
*Oceanogr.*, 44(7), 1599–1608. 839  
 Fujita, Y., A. Murakami, K. Aizawa, and K. Ohki (1994), Short-term and 840  
 long-term adaptation of the photosynthetic apparatus: Homeostatic prop- 841  
 erties of thylakoids, in *The Molecular Biology of Cyanobacteria*, edited 842  
 by D. A. Bryant, pp. 677–692, Kluwer Acad., Norwell, Mass. 843  
 Glenn, S. M., M. F. Crowley, D. B. Haidvogel, and Y. T. Song (1996), 844  
 Underwater observatory captures coastal upwelling events off New 845  
 Jersey, *Eos Trans. AGU*, 77, 233–236. 846

- 847 Glenn, S. M., T. D. Dickey, W. P. Bisset, and O. Schofield (2000), Long-  
848 term real-time coastal ocean observation networks, *Oceanography*, 13,  
849 24–34.
- 850 Gong, G., J. Chang, and Y. Wen (1999), Estimation of primary production  
851 in the Kuroshio waters northeast of Taiwan using a photosynthetic-  
852 irradiance model, *Deep Sea Res., Part I*, 46, 93–108.
- 853 Gordon, H. R., and A. Morel (1983), *Remote Sensing of Ocean Color for*  
854 *Interpretation of Satellite Visible Imagery: A Review*, Springer-Verlag,  
855 New York.
- 856 Hallegraeff, G. M. (1993), A review of harmful algal blooms and their  
857 apparent global increase, *Phycology*, 32, 79–99.
- 858 Hoepffner, N., and S. Sathyendranath (1992), Bio-optical characteristics of  
859 coastal waters: Absorption spectra of phytoplankton and pigment distri-  
860 bution in the western North Atlantic, *Limnol. Oceanogr.*, 37(8), 1660–  
861 1679.
- 862 Holligan, P. M., and W. A. Reiners (1992), Predicting the responses of the  
863 coastal zone to global change, *Adv. Ecol. Res.*, 22, 211–221.
- 864 Jassby, A. D., and T. Platt (1976), Mathematical formulation of the relation-  
865 ship between photosynthesis and light for phytoplankton, *Limnol.*  
866 *Oceanogr.*, 21, 540–547.
- 867 Jickells, J. D. (1998), Nutrient biogeochemistry of the coastal zone,  
868 *Science*, 281, 217–222.
- 869 Johnsen, G., O. Samsø, L. Granskog, and E. Sakshaug (1994), In vivo  
870 absorption characteristics in 10 classes of bloom-forming phytoplankton:  
871 Taxonomic characteristics and responses to photoadaptation by means to  
872 discriminant and HPLC analysis, *Mar. Ecol. Prog. Ser.*, 105, 149–157.
- 873 Johnson, D. R., J. Miller, and O. Schofield (2003), Dynamics and optics of  
874 the Hudson River outflow plume, *J. Geophys. Res.*, 108(C10), 3323,  
875 doi:10.1029/2002JC001485.
- 876 Kishino, M., M. Takahashi, N. Okami, and S. Ichimura (1985), Estimation  
877 of the spectral absorption coefficients of phytoplankton in the sea, *Bull.*  
878 *Mar. Sci.*, 37(2), 634–642.
- 879 Kolber, Z. S., and P. G. Falkowski (1993), Use of active fluorescence to  
880 estimate phytoplankton photosynthesis in situ, *Limnol. Oceanogr.*, 38,  
881 1646–1665.
- 882 Kolber, Z. S., J. Zehr, and P. G. Falkowski (1988), Effects of growth  
883 irradiance and nitrogen limitation on photosynthetic energy conversion  
884 in photosystem II, *Plant Physiol.*, 88, 923–929.
- 885 Kroon, B. M. A., and N. A. Dijkman (1996), Photosystem II quantum  
886 yields, off-line measured *P/I* parameters and carbohydrate dynamics in  
887 *Chlorella vulgaris* grown under a fluctuating light regime and its  
888 application for optimizing mass cultures, *J. Appl. Phycol.*, 8(4–5),  
889 313–323.
- 890 Kyewalyanga, M. N., T. Platt, S. Sathyendranath, V. A. Lutz, and V. Stuart  
891 (1998), Seasonal variations in physiological parameters of phytoplankton  
892 across the North Atlantic, *J. Plankton Res.*, 20(1), 17–42.
- 893 Laws, E. A. (1991), Photosynthetic quotients, new production and net  
894 community production in the open ocean, *Deep Sea Res., Part A*, 38,  
895 143–167.
- 896 Lewis, M. R., O. Ulloa, and T. Platt (1988), Photosynthetic action, absorp-  
897 tion, and quantum yield spectra for a natural population of *Oscillatoria*  
898 in the North Atlantic, *Limnol. Oceanogr.*, 33(1), 92–98.
- 899 Lindley, S. T., R. R. Bidigare, and R. T. Barber (1995), Phytoplankton  
900 photosynthesis parameters along 140°W in the equatorial Pacific, *Deep*  
901 *Sea Res., Part II*, 42(2–3), 441–463.
- 902 Lorenzo, L. M., B. Arbones, F. G. Figueiras, G. H. Tilstone, and F. L.  
903 Figueroa (2002), Photosynthesis, primary production and phytoplankton  
904 growth rates in Gerlache and Bransfield Straits during Austral summer:  
905 Cruise of FRUELA 95, *Deep Sea Res., Part II*, 49, 707–721.
- 906 Marra, J. (1993), Proportionality between in situ carbon assimilation and  
907 bio-optical measures of primary production in the Gulf of Maine in  
908 summer, *Limnol. Oceanogr.*, 38(1), 232–238.
- 909 Marra, J., C. C. Trees, R. R. Bidigare, and R. T. Barber (2000), Pigment  
910 absorption and quantum yields in the Arabian Sea, *Deep Sea Res., Part II*,  
911 47, 1279–1299.
- 912 Moline, M., and B. B. Prézélin (1996), Long-term monitoring and analy-  
913 sis of physical factors regulating variability in coastal Antarctic phyto-  
914 plankton biomass, in situ productivity and taxonomic composition over  
915 subseasonal, seasonal and interannual time scales, *Mar. Ecol. Prog. Ser.*,  
916 145, 143–160.
- 917 Moline, M. A., O. Schofield, and N. P. Boucher (1998), Photosynthetic  
918 parameters and empirical modeling of primary production: A case study  
919 on the Antarctic Peninsula shelf, *Antarct. Sci.*, 10(1), 45–54.
- 920 Morel, A., and L. Prieur (1977), Analysis of variations in ocean color,  
921 *Limnol. Oceanogr.*, 22, 709–722.
- 922 Morel, A., D. Antoine, M. Babin, and Y. Dandonneau (1996), Measured  
923 and modeled primary production in the northeast Atlantic (EUMELI  
924 JGOFS program): The impact of natural variations in photosynthetic  
925 parameters in model predictive skill, *Deep Sea Res., Part II*, 43,  
926 1273–1304.
- Ondrusek, M. E., R. R. Bidigare, K. Waters, and D. M. Karl (2001), A  
927 predictive model for estimating rates of primary production in the sub-  
928 tropical North Pacific Ocean, *Deep Sea Res., Part II*, 48, 1837–1863.  
929
- Pope, R., and E. Fry (1997), Absorption spectrum (380–700 nm) of pure  
930 water, II, Integrating cavity measurements, *Appl. Opt.*, 36(33), 8710–  
931 8723.
- Prézélin, B. B. (1991), Diel periodicity in phytoplankton productivity,  
932 *Hydrobiology*, 238, 1–35.
- Prézélin, B. B., and B. A. Boczar (1986), Molecular bases of cell absorption  
933 and fluorescence in phytoplankton: Potential applications to studies in  
934 optical oceanography, *Prog. Phycol. Res.*, 4, 349–464.
- Prézélin, B. B., R. R. Bidigare, H. A. Matlick, M. Putt, and B. VerHoven  
935 (1987), Diurnal patterns of size-fractionated primary productivity across a  
936 coastal front, *Biol. Morya Vladivostok*, 96, 563–574.
- Prézélin, B. B., H. E. Glover, B. VerHoeven, D. K. Steinberg, H. A.  
937 Matlick, O. Schofield, N. B. Nelson, M. Wyamn, and L. Campbell  
938 (1989), Blue-green light effects on light-limited rates of photosynthesis:  
939 Relationship to pigmentation and productivity estimates from the Sargasso  
940 Sea, *Mar. Ecol. Prog. Ser.*, 54, 121–136.
- Ryther, J. H., and D. W. Menzel (1959), Light adaptation by marine phy-  
941 toplankton, *Limnol. Oceanogr.*, 4(4), 492–497.
- Sakshaug, E., A. Bricaud, Y. Dandonneau, P. G. Falkowski, D. A. Kiefer,  
942 L. Legendre, A. Morel, J. Parslow, and M. Takahashi (1997), Parameters  
943 of photosynthesis: Definitions, theory and interpretation of results,  
944 *J. Plankton Res.*, 19(11), 1637–1670.
- Sathyendranath, S., V. Stuart, B. D. Irwin, H. Maass, G. Savidge, L. Gilpin,  
945 and T. Platt (1999), Seasonal variations in bio-optical properties of phy-  
946 toplankton in the Arabian Sea, *Deep Sea Res., Part II*, 46, 633–653.
- Schofield, O., B. B. Prézélin, R. R. Bidigare, and R. C. Smith (1993), In  
947 situ photosynthetic quantum yield, correspondence to hydrographic and  
948 optical variability within the southern California Bight, *Mar. Ecol. Prog.*  
949 *Ser.*, 93, 24–37.
- Schofield, O., B. B. Prézélin, and G. Johnsen (1996), Wavelength depen-  
950 dency in photosynthetic parameters for two dinoflagellate species  
951 *Heterocapsa pygmaea* and *Prorocentrum minimum*: Implications for  
952 the bio-optical modeling of photosynthetic rates, *J. Phycol.*, 32, 574–583.
- Schofield, O., T. Bergmann, W. P. Bisset, F. Grassle, D. Haidvogel,  
953 J. Kohut, M. Moline, and S. Glenn (2002), The long term ecosystem  
954 observatory: An integrated coastal observatory, *IEEE J. Oceanic Eng.*,  
955 27(2), 146–154.
- Siegel, D. A., et al. (2001), Bio-optical modeling of primary production on  
956 regional scales: The Bermuda bio-optics project, *Deep Sea Res., Part II*,  
957 48, 1865–1896.
- Smith, R. C., B. B. Prézélin, R. R. Bidigare, and K. S. Baker (1989), Bio-  
958 optical modeling of photosynthetic production in coastal waters, *Limnol.*  
959 *Oceanogr.*, 38(4), 1524–1544.
- Sosik, H. M. (1996), Bio-optical modeling of primary production: Conse-  
960 quences of variability in quantum yield and specific absorption, *Mar.*  
961 *Ecol. Prog. Ser.*, 143, 225–238.
- Sournia, A. (1974), Circadian periodicities in natural populations of marine  
962 phytoplankton: A review, *Adv. Mar. Biol.*, 6, 325–389.
- Stramski, D., and A. Morel (1990), Optical properties of photosynthetic  
963 picoplankton in different physiological states as affected by growth irra-  
964 diance, *Deep Sea Res.*, 37, 245–266.
- Vodacek, A., N. V. Blough, M. D. DeGrandpre, E. T. Peltzer, and R. K.  
965 Nelson (1997), Seasonal variation of CDOM and DOC in the middle  
966 Atlantic Bight: Terrestrial inputs and photooxidation, *Limnol. Oceanogr.*,  
967 42(4), 674–686.
- Walsh, J. J. (1978), Wind events and food chain dynamics within the New  
968 York Bight, *Limnol. Oceanogr.*, 23(4), 649–683.
- Ward, J. H. (1963), Hierarchical grouping to optimize an objective function,  
969 *J. Am. Stat. Assoc.*, 58, 236–244.
- Waters, K. J., R. C. Smith, and J. Marra (1994), Phytoplankton production  
970 in the Sargasso Sea as determined using optical mooring data, *J. Geo-*  
971 *phys. Res.*, 99(C9), 18,385–18,402.
- Wright, S. W., S. W. Jeffrey, R. F. C. Mantoura, C. A. Llewellyn,  
972 T. Bjornland, D. Repeta, and N. Welschmeyer (1991), Improved HPLC  
973 method for the analysis of chlorophylls and carotenoids from marine  
974 phytoplankton, *Mar. Ecol. Prog. Ser.*, 77, 183–196.
- Zimmerman, R. C., J. B. SooHoo, J. N. Kremer, and D. Z. D'Argenio  
975 (1987), Evaluation of variance approximation techniques of non-linear  
976 photosynthetic-irradiance models, *Biol. Morya Vladivostok*, 95, 209–215.  
977

T. Bergmann, S. Glenn, M. J. Oliver, and O. Schofield, Institute of  
Marine and Coastal Sciences, Rutgers University, 71 Dudley Road, New  
Brunswick, NJ 08903, USA. (oliver@imcs.rutgers.edu)  
M. Moline and C. Orrico, Biological Sciences Department, California  
Polytechnic State University, San Luis Obispo, CA 93407, USA.